ARTICLE

Spectral Analysis of Multiplex Raman Probe Signatures

Barry R. Lutz,[†] Claire E. Dentinger,[†] Lienchi N. Nguyen,[†] Lei Sun,[†] Jingwu Zhang,[†] April N. Allen,[‡] Selena Chan,[†,*] and Beatrice S. Knudsen[‡,*]

[†]Biomedical/Life Sciences, Digital Health Group, Intel Corporation, SC3-41 2200 Mission College Boulevard, Santa Clara, California 95054, and [‡]Division of Public Health Sciences, Fred Hutchinson Cancer Research Center, M5-A864, 1212 Aloha Street, Seattle, Washington 98109

ABSTRACT Raman nanoparticle probes are an emerging new class of optical labels for interrogation of physiological and pathological processes in bioassays, cells, and tissues. Although their unique emission signatures are ideal for multiplexing, the full potential of these probes has not been realized because conventional analysis methods are inadequate. We report a novel spectral fitting method that exploits the entire spectral signature to quantitatively extract individual probe signals from multiplex spectra. We evaluate the method in a series of multiplex assays using unconjugated and antibody-conjugated composite organic−inorganic nanoparticles (COINs). Results show sensitive multiplex detection of small signals (<2% of total signal) and similar detection limits in corresponding 4-plex and singlet plate binding assays. In a triplex assay on formalin-fixed human prostate tissue, two antibody-conjugated COINs and a conventional fluorophore are used to image expression of prostate-specific antigen, cytokeratin-18, and DNA. The spectral analysis method effectively removes tissue autofluorescence and other unknown background, allowing accurate and reproducible imaging (area under ROC curve 0.89 ± 0.03) at subcellular spatial resolution. In all assay systems, the error attributable to spectral analysis constitutes ≤2% of total signal. The spectral fitting method provides (1) quantification of signals from multiplex spectra with overlapping peaks, (2) robust spot-by-spot removal of unknown background, (3) the opportunity to quantitatively assess the analysis error, (4) elimination of operator bias, and (5) simple automation appropriate for high-throughput analysis. The simple implementation and universal applicability of this approach significantly expands the potential of Raman probes for quantitative *in vivo* and *ex vivo* multiplex analysis.

KEYWORDS: composite organic−inorganic nanoparticles (COINs) · surface-enhanced Raman scattering (SERS) · multiplex assays · tissue imaging · prostate-specific antigen · cytokeratin-18

Methods for simultaneous detection of multiple targets are critical for analysis of biological samples. With the rapidly increasing biological understanding, there are enormous opportunities to extract information about cellular and molecular processes from biological specimens. However, detection methods pose a major limitation. One of the main challenges is to measure multiple biomarkers simultaneously using a multiplex system. This approach greatly reduces the amount of precious samples that are needed for analysis, as well as the time and cost of the measurement, and facilitates interpretation of signals with nonuniform distribution throughout the specimen. Co-localization and spatial resolution of signals permit accurate analysis of heterogeneous biological samples in applications such as cell and animal imaging, tissue histology, and flow cytometry. Commonly used fluorescent dyes or quantum dots face significant limitations in multiplexing applications due to the interference from tissue autofluorescence and the overlap of emission peaks.

Nanoparticle probes utilizing surface-enhanced Raman scattering (SERS) emit unique spectral signatures with narrow peaks that are ideal for multiplexing. Raman emission is normally extremely weak compared to fluorescence, but enormous signal enhancements can be created by adsorbing Raman-active molecules onto roughened metal surfaces[1−3] or nanoparticles.[4] In 1997,[5,6] it was demonstrated that nanoparticle-enhanced SERS emission could be as bright as fluorescence, and this initiated development of a new class of optical probes for biomolecule detection. Rapid development of fabrication and biomolecule conjugation methods expanded their applications in immunoassays,[7−13] nucleic acid hybridization,[14−21] cell and tissue staining,[8,13,22−26] and *in vivo* imaging.[27] Despite the significant potential of Raman probes for improved multiplex quantification, they have primarily been used for qualitative detection of single targets. Notable field-advancing biological applications include highly sensitive detection of single DNA targets,[15,28] detection and quantification of five to six DNA targets,[17−19] sensitive detection of virus and proteins in plate binding assays,[9,11] duplex protein detection in cells,[25] and a recent demonstration of *in vivo* targeting and imaging.[27] The data analysis in these assays relies on qualitative observations, or

*Address correspondence to bknudsen@fhcrc.org, selena.chan@intel.com.

Received for review April 24, 2008 and accepted October 03, 2008.

Published online November 4, 2008. 10.1021/nn800243g CCC: $40.75

on quantitation based on a single characteristic peak, and discards important spectral information encoded in the complex, multipeak Raman signature. Spectral fitting using reference spectra has been applied to improve multiplexing of fluorophores[29] but has not yet been applied to analysis of Raman probe signatures.

Here we report a simple multiplex spectral fitting method that exploits the entire fingerprint to separate and quantify individual Raman probe signals. We previously applied the spectral fitting approach to image single protein expression in tissues and found that it effectively separates probe signals from autofluorescence.[8,13] In these studies, Raman probes were compared for accuracy and sensitivity with conventional fluorophores.[13] In the current study, we specifically address the analysis of Raman data from multiplex probe systems and evaluate the performance of a novel spectral deconvolution method in various multiplex settings. This spectral fitting method, which is exceedingly simple to implement and amenable to high-throughput analysis, can be applied to any multiplex system of Raman probes.

RESULTS AND DISCUSSION

COIN Fabrication. A variety of fabrication approaches have been reported using different Raman labels, nanoparticle materials, encapsulation methods, and conjugation methods.[30] Composite organic−inorganic nanoparticles (COINs) developed by our group[7,8,13] take advantage of superior enhancement through aggregation with silver nanoparticles, allow the use of a broad range of different Raman active molecules, and possess a biocompatible surface coating for conjugation to a variety of detection probes. Figure 1A illustrates the fabrication, encapsulation, and functionalization of COIN probes. Silver nanoparticles are aggregated in the presence of organic Raman-active molecules, such as conventional colorimetric or fluorescent dyes. BSA coating shields Raman labels from the environment, preserves their signatures, reduces nonspecific interactions with bioactive surfaces, and permits a simple one-step conjugation to detection probes,[8] such as antibodies or nucleic acids.

Spectral Characteristics of COINs. Figure 1B shows the Raman signature for a COIN that contains the common dye molecule, basic fuschin, as the Raman label (BFU-COIN). Each peak in the COIN spectrum originates from specific vibrational modes of basic fuschin. Figure 1B directly compares the emission spectra of BFU-COIN, Qdot 565, and Alexa 555. The peaks of Raman emission (~2 nm) are much narrower than the single peak fluorescence emission from molecular fluorophores (40−50 nm) or quantum dots (30−40 nm). Although fluorescent probes with a wide range of emission colors are available, multiplexing using fluorophores is restricted by the overlap in emission peaks and the difficulty of separating true probe signals from background.

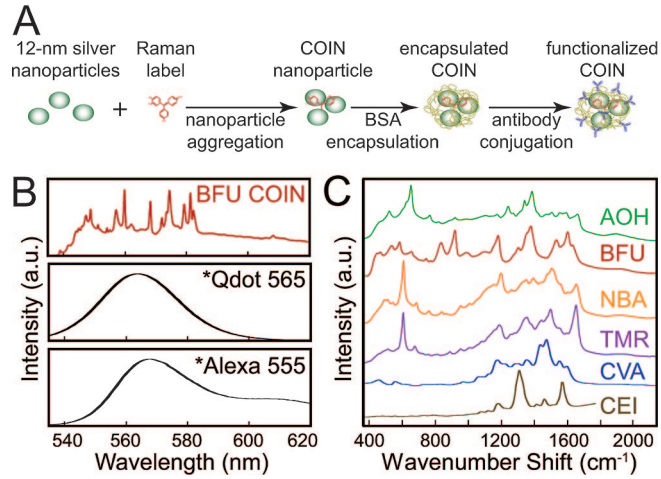

Figure 1. Fabrication and spectral characteristics of COINs. (A) Schematic of COIN fabrication, encapsulation, and antibody conjugation. Functionalized COINs are ~60 nm in diameter. (B) Comparison of emission spectra for COIN (532 nm excitation), Qdot, and a molecular fluorophore (*spectra reproduced with permission from Invitrogen Inc., www.probes.invitrogen.com). (C) Reference spectra of individual COINs excited by a green laser.

In comparison, the sharp peaks and complex spectral fingerprints of Raman emission readily distinguish individual probe signatures and facilitate their separation from background. Raman nanoparticle probes possess diverse and complex spectral characteristics for multiplexing, an inherent resistance to photobleaching, decreased toxicity compared to quantum dots, and an unlimited potential for creation of new probes with numerous Raman-active substances.[30]

Figure 1C shows Raman spectra of the six COINs used in this work; the Raman labels are acridin orange (AOH), basic fuschin (BFU), Nile blue A (NBA), tetramethyl rhodamine isothiocyanate (TMR), cresyl violet (CVA), and 1,1′-diethyl-2,2′-cyanine (CEI). Unlike fluorescent emission, Raman peaks are always located at a fixed energy shift away from the chosen laser excitation wavelength (*i.e.*, wavenumber shift = $1/wl$(emission) − $1/wl$(excitation)). Excitation of COINs with a green laser produces characteristic emission spectra in the green-orange wavelength region.

Deconvolution of Multiplex Raman Spectra. Despite excellent work in development of Raman probes and biomolecule assays, applications that truly explore the potential for quantitative multiplexing have been rare. This can be attributed to the lack of an appropriate analysis method that takes advantage of the complex signature often cited as the major advantage of Raman probes. We developed a simple fitting method that exploits the entire spectral fingerprint to quantitatively extract signals from multiplex Raman spectra (Figure 2). Figure 2A shows a multiplex spectrum emitted by a combination of two COINs. The spectrum is deconvoluted by least-squares regression using archived pure COIN reference spectra (Figure 2B), a representative background spectrum, and freely varying polynomial

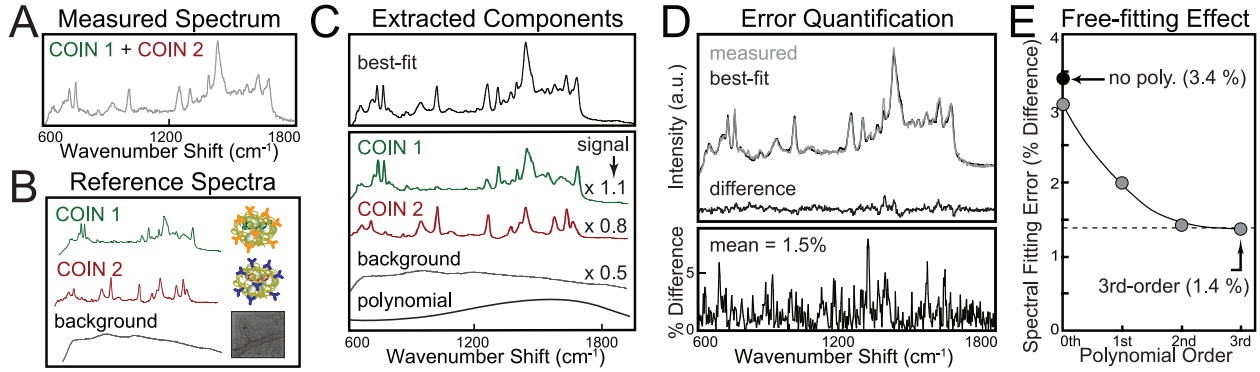

Figure 2. Spectral fitting method for quantifying signals from multiplex spectra. (A) Spectrum from a duplex assay on tissue using antibody-conjugated COIN. (B) Pure COIN reference spectra and a representative reference spectrum of tissue autofluorescence. (C) Total spectrum (upper panel), pure component spectra of individual COINs, autofluorescence, and a free fitting polynomial extracted from the measured spectrum by least-squares regression. The pure component signals of individual COINs are determined from the intensity ratio of the extracted and reference spectra. (D and E) Spectral fitting error. (D) The best-fit spectrum is subtracted from the measured spectrum (upper panel) and the difference normalized to the signal intensity (lower panel). The spectral fitting error is defined as the average percent difference between measured and best-fit spectra and calculated across the entire wavelength range of the COIN fingerprint. (E) Optimization of the free-fitting polynomial to reduce the quantification error. A 532 nm laser was used as the excitation source.

components (see Methods). The mean peak height of each reference spectrum is normalized to allow direct comparison of signal intensities between extracted pure component spectra. All components are simultaneously varied in magnitude to provide the best fit to the measured spectrum. For purposes of quantification, each probe signal is reported as the magnitude of its extracted spectrum relative to its reference spectrum (Figure 2C).

Figure 2D shows that the resulting best-fit spectrum (black) is nearly indistinguishable from the measured spectrum (gray). The spectral fitting error is calculated as the mean percent difference between measured and best-fit spectra across the wavelength range of the COIN signature (Figure 2D, bottom). The spectral fitting error provides a direct measure of the signal quantification error that is attributable to fitting algorithm and essentially monitors the quality of individual spectral fits.

A major challenge for quantitation of signals from biological samples is the interference of intrinsic autofluorescence. To reduce autofluorescence emission, it is common to use Raman probes optimized for red or near-infrared excitation, but this restriction uses only a small portion of the visible window and limits the number of probes that can be multiplexed. The COINs used here are optimized for green laser excitation,[7] which complements probes designed for long-wavelength excitation but also results in significant autofluorescence emission from biological samples. The ability to quantitatively separate probe signals from autofluorescence further increases the order of multiplexing by allowing applications of probe sets excited at different wavelengths across the across the visible spectrum.

Figure 2B (bottom) shows a representative autofluorescence spectrum for an unstained tissue section excited by a green laser. The Raman signatures from tissue proteins are too small to be detected, and the tissue emission is dominated by a broad fluorescence background emanating from fibrillar proteins. Because the background emission often varies across areas in a sample, subtracting a single representative background spectrum could result in miscalculating probe signals. This is taken into account in our fitting method, which does not require an *a priori* subtraction of background. The representative autofluorescence spectrum is included as a reference spectrum in our analysis, and it is free to vary in magnitude for each measurement point. A unique aspect of the method is the addition of polynomial components that are also free to vary in magnitude and shape during the fitting procedure (Figure S1 in the Supporting Information). These account for variation in spectral character of background signal, including autofluorescence and other sources (*e.g.*, intense particle scattering, fluorescent debris).

Figure 2E shows that including the free-fitting polynomial components in analysis of tissue samples reduces the spectral fitting error by 2−3-fold. Error levels reach a minimum at ~1.4% of total intensity for polynomials second-order or higher; a third-order polynomial was used for subsequent spectral analyses. In all of our experiments under different conditions (different COIN labels, multiplex COIN combinations, signal intensities) and assay formats (solution, plate, and tissue assays), the fitting error remained between 1 and 2% of the total signal intensity.

In the experiments presented below, we explore the quantitative aspects of spectral analysis under different multiplex conditions and demonstrate multiplex imaging of a complex biological sample. The insight gained through these experiments applies in general to Raman probes, and the methods can be easily adopted to improve quantitation in any multiplex Raman probe system.

Multiplex Detection of Low-Abundance Signals. Regardless of probe type, multiplexing inherently reduces the abil-

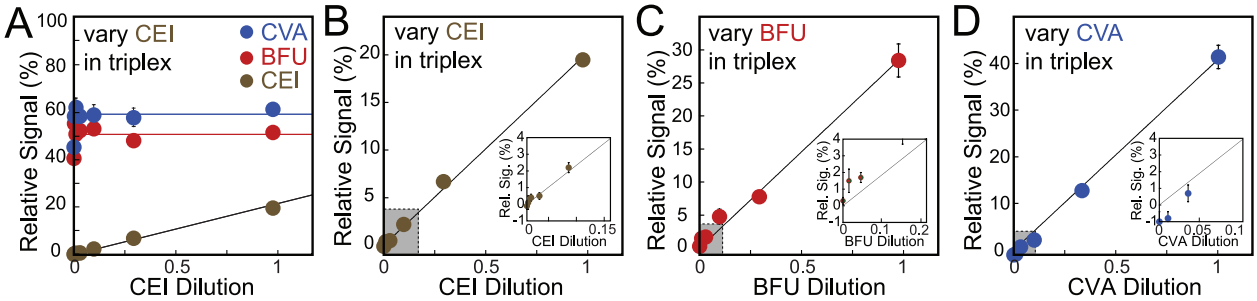

Figure 3. Limit of detection of COIN signals in a triplex solution measurement. Three unconjugated COINs were mixed in solution, and pure component signals for each COIN were quantified by the spectral fitting method. (A) Detection of CEI COIN in the presence of high intensity CVA and BFU COIN signals. CVA-COIN and BFU-COIN are held at constant concentrations (red and blue), while the CEI COIN is serially diluted (*x*-axis). Relative signal intensities on the *y*-axis are reported as the percent of combined signal of the nonvaried COINs (CVA and BFU). (B−D) Each panel represents a separate triplex dilution experiment varying a single COIN (CEI, BFU, or CVA). Two COINs are held at a constant high concentration and not included in the panel because their signals are off the scale, while the third COIN is serially diluted. The gray boxes are expanded in the inset plots to evaluate the limit of detection. Error bars are one standard deviation of the mean, and some are smaller than plotted symbols ($n = 100$). A 514 nm laser was used to excite COIN. The statistical data analysis is detailed in Table S1 in the Supporting Information.

ity to detect low-abundance analytes and weak probes since their signals are generally masked by probes with high signal intensities. In the reported multiplex experiments, the spectral fitting error is a fixed percentage of total signal, and the limit of detection (LOD) of individual probes is expected to be proportional to the total signal. We designed a simple experiment using unconjugated COINs in solution to isolate the effect of the spectral fitting error on the detection sensitivity and to eliminate other error contributions. In Figure 3A, two COINs are held at constant high probe intensity levels (blue, red), while the third COIN (brown) is serially diluted to determine its LOD in the triplex measurement. The individual COIN signals are extracted by spectral analysis, and the signal is reported as a proportion of the summed signals from the two nonvaried COINs. Figure 3B−D shows the titration response for serial dilutions of three COINs, and insets depict detail at low signal levels. The LOD is defined as three times the standard deviation above the zero point. For three separate experiments varying CEI, BFU, and CVA COINs, the LOD is 0.6, 0.9, and 1.7% of total signal, respectively, which is consistent with the spectral fitting error for this experiment (~2% of total signal). In each case, the low-abundance COIN is detectable at signal levels that are 50−100-fold smaller than the total signal. Thus, the spectral fitting method performs exceptionally well in multiplex systems for detecting low-abundance probe signals.

Quantitative Multiplex Detection of Antibody-Conjugated Probes.

In preparation for tissue imaging, we tested four antibody-conjugated COINs in a quadruplex plate binding assay detecting prostate-specific antigen (PSA). We prepared four different Ab-COIN probes by conjugation to a single source of anti-PSA antibody to reduce sources of error caused by antibody affinity and nonspecific binding. A mixture of four probes at a fixed concentration was added to wells coated with a serial dilution of purified PSA protein (Figure 4). Figure 4A shows the spectral deconvolution for one well. The best-fit spectrum (black) is overlaid on the measured spectrum (gray) and contains signatures of all four Ab-COINs. Isolated peaks arising from a single COIN are indicated by colored arrows, and peaks arising from multiple COINs are indicated by colored boxes. Two of the four COINs cannot be identified by unique peaks due to spectral

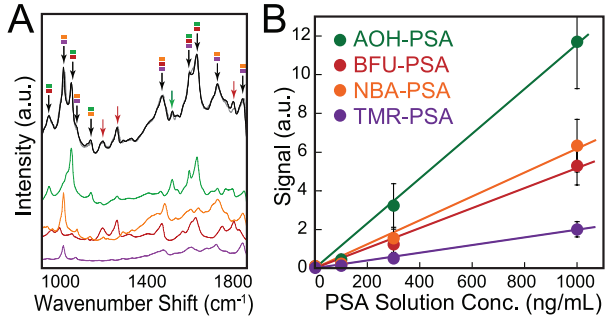

C LOD for COINs in singlet or quadruplex assays (ng/mL)

COIN	singlet	4-plex
AOH	26 ± 4	28 ± 3
BFU	30 ± 4	43 ± 4
NBA	42 ± 1	36 ± 4
TMR	38 ± 3	45 ± 6

Figure 4. Quadruplex PSA plate binding assay using antibody-conjugated COINs. (A) Spectral deconvolution of the quadruplex assay. The upper traces represent the measured spectrum (gray) and best-fit (black) spectrum. The colored lines represent the pure COIN spectra extracted with the spectral deconvolution method. Peaks that primarily arise from a single COIN are shown by colored arrows, and peaks arising from multiple COINs are color coded by boxes. (B) Dose−response curves for the multiplex plate binding assay using four COIN preparations conjugated to anti-PSA antibody. The four COIN−Ab conjugates were mixed together at fixed concentrations before addition to wells, and the pure component signals were quantified by the spectral fitting method. The *x*-axis shows the PSA solution concentrations adsorbed onto the aldehyde surface of each well (see Methods). Colored lines are the best-fit dose−response curves, and error bars are standard deviations from two assays. (C) Comparison of limits of detection (LOD) for singlet and quadruplex PSA plate binding assays using the set of four COINs. Values shown are the mean and one standard deviation. Singlet and quadruplex LODs are not statistically different at $p < 0.05$. Corresponding singlet assays are shown in Figure S2 in the Supporting Information, and detailed statistics for the experiments are given in Table S2 in the Supporting Information. A 514 nm laser was used to excite COIN.

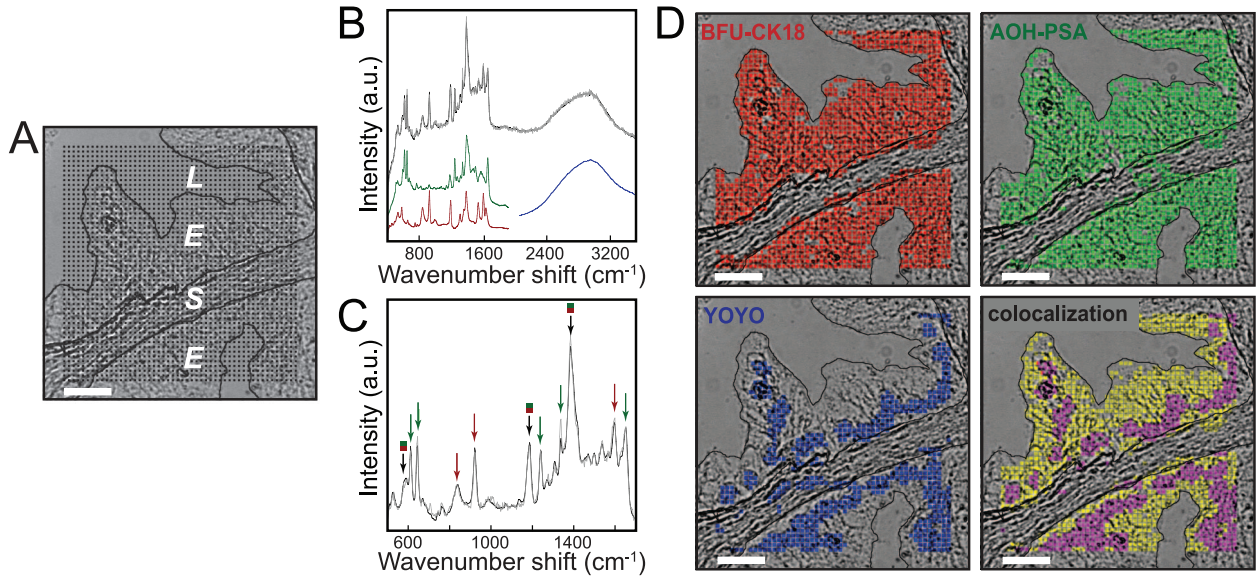

Figure 5. Spectral deconvolution in a multiplex FFPE tissue assay. BFU−COIN was conjugated to anti-CK18 antibody (BFU−CK18); AOH−COIN was conjugated to anti-PSA antibody (AOH−PSA), and a fluorescent dye targeted DNA (YOYO). The pure component signals were quantified by the spectral fitting method. (A) Brightfield image of prostate tissue. Spectra were recorded at each spot in a raster pattern (50 × 50, 1 μm spacing, small black spots). The raster spans epithelia (E) of two prostate glands, a narrow band of stromal tissue separating the glands (S), and the gland lumen (L). (B) Spectral deconvolution for a single spot measurement. Upper traces represent the measured spectrum (gray) and best-fit spectrum (black). Colored lines represent extracted spectra for BFU−CK18 (red), AOH−PSA (green), and YOYO (blue). (C) Detail of the COIN fitting region showing measured (gray) and best-fit (black) spectra. Arrows indicate unique peaks from BFU (red) and AOH (green) COINs, and peaks arising from both COINs are indicated by colored boxes. The spectral fitting error of the pictured spectrum is 1.2% of total signal. (D) Pure component images and co-localization image of the three probes. Pure component images report positive and negative signals in each spot of the raster using an intensity threshold for individual probes (see Methods). DNA is visualized with the YOYO nucleic acid stain and marked in blue; COIN signals of CK18 are marked in red and PSA in green. The co-localization image identifies epithelial nuclei (magenta) and coexpression of CK18 and PSA specifically in the epithelium (yellow). Summary statistics for staining quality in repeated triplex assays are given in Table S3 in the Supporting Information. Scale bars, 10 μm. A 532 nm laser was used as the excitation source.

overlap, demonstrating that the typical single peak method cannot be used for quantification. The spectral fitting method exploits the entire spectral signature to extract individual component spectra (Figure 4A, colored) and quantitative signals for each Ab-COIN. The extracted signals from the quadruplex analysis are used to construct dose−response curves shown in Figure 4B for the four antibody−COIN conjugates. The extracted signals represent true probe intensities, and the difference between probes reflects inherent signal intensities of the different COINs. We previously reported the saturability of the dose response curve,[13] suggesting that the observed antibody binding is specific. For all data points in Figure 4B, the intensity of individual Ab-COINs is proportional to the coated PSA concentration ($R^2 > 0.98$) and comparable to the linear Ab-COIN dose−response in singlet experiments (Figure S2 in the Supporting Information).

In contrast to the solution assay, the LOD of the plate binding assay is affected by nonspecific binding of the antibody. In Figure 4B, the four Ab−COINs show similar amounts of nonspecific signal (<0.11 au). The LOD for individual Ab−COINs was defined as three standard deviations above the mean signal intensity in the blank wells. Figure 4C compares the LODs for each Ab−COIN measured in quadruplex and singlet experiments. We do not observe a statistically significant difference, suggesting that multiplexing does not change the LOD of the Ab−COINs. As with the other assays, the spectral fitting error in this experiment was a constant percentage of total signal for all singlet and quadruplex assays (~1% of total signal). Thus, the absolute error from the analysis is larger in the multiplex experiments due to larger combined signal from all probes. In this experiment, multiplexing does not affect the LOD because the spectral fitting error is relatively small compared to the major component of the error, which is caused by the nonspecific binding of the antibody (Table S2 in the Supporting Information). Together, these results suggest that spectral fitting allows multiplexing of at least four probes without compromising quantification.

Detection of Protein Expression in Formalin-Fixed and Paraffin-Embedded Tissues. As a multiplexing application of clinical relevance, we applied the spectral fitting method to image the expression of proteins in formalin-fixed paraffin-embedded (FFPE) prostate tissue sections. Five micrometer thick tissues were probed simultaneously with two antibody-conjugated COINs and a fluorescent nucleic acid stain. BFU was conjugated to anticytokeratin-18 (BFU−CK18), and AOH was conjugated to anti-PSA antibody (AOH−PSA). After loosening the tissue by enzymatic digestion, BFU−CK18 and AOH−PSA antibody conjugates were simultaneously

incubated with the tissue section on a glass slide. The tissue was washed to remove unbound Ab−COINs, followed by treatment with the YOYO nucleic acid stain.

Multiplex spectra were recorded in a raster pattern of 2500 spots (Figure 5A). The maximum image resolution using the raster scanning method is set by the beam spot size (~1 μm). The total scan time includes the sum of acquisition times for each spot (0.1 s per spot, ~4 min) and the time required to move the stage between each point (~15 min total scan time). Improved image resolution and decreased scan time could be achieved by commonly used tunable filters that record entire images at specified wavelengths to build an equivalent data set (*i.e.*, the hyperspectral data cube). The time required for acquisition is not affected by the number of probes used, although longer acquisition times will improve the signal-to-noise ratio and spectral deconvolution accuracy for higher order multiplexing. The location of the raster was chosen to encompass an area of prostate epithelium (E), known to express PSA and CK18 proteins (see Figure S3 in the Supporting Information), and areas of the prostate stroma (S) and the lumen within prostate glands (L), where antibody binding is not expected.

Figure 5B shows a multiplex spectrum measured at one spot of the raster using a single laser for excitation (532 nm). The COIN spectra overlap and are separated from the fluorescent emission spectrum of the YOYO dye. The spectral analysis included probe reference spectra (BFU, AOH, and YOYO), a representative autofluorescence spectrum from a different tissue sample, and freely varying polynomial components. Figure 5B shows the measured spectrum (gray), the resulting best-fit spectrum (black), and the extracted pure probe spectra (colored). Figure 5C shows that each peak in the spectrum is accurately fit by the reference spectra, despite increased noise due to short acquisition times (0.1 s per spot). The spectral fitting error for triplex tissue experiments was only 1−2% of total signal, which is as low as that for the solution and plate binding assays (Figures 3 and 4). This result clearly demonstrates that the spectral fitting method overcomes the problem of autofluorescence that often interferes with protein measurements in biological samples.

To visualize the expression of proteins and the location of nuclear DNA in the context of tissue morphology, the extracted pure component signals are mapped onto the tissue image. Figure 5D shows the pure component images for CK18−BFU, PSA−AOH, and YOYO. The pure component signals at each spot are used to classify the spot as positive (colored pixel) or negative (gray pixel) for the corresponding target. The image shows the expected epithelial coexpression of CK18 and PSA and clear identification of nuclei in both the epithelium and stroma (YOYO). No steric interference was observed between the CK18 and PSA probes (Figure S4 in the Supporting Information). The accuracy of protein detection compares with our previous work[13] using COIN for single-antigen detection (Table S3 in the Supporting Information).

The multiplex tissue imaging with COIN−antibody conjugates demonstrates the feasibility of using spectral analysis for simultaneous detection of at least two proteins and DNA in tissues. This system highlights the major strengths of the spectral deconvolution method, which can be generalized to other applications of Raman spectroscopy, such as small animal imaging and high-throughput multiplex analysis in array and cell-based platforms.

The spectral fitting method presented here greatly increases the power for multiplex quantification compared to commonly used peak identification methods. In experiments with three- or four-probe combinations (Figure 3 and Figure 4), simple peak measurement methods are not possible because characteristic probe-specific peaks cannot be identified. Further, we include a free-fitting component that compensates for unknown background without the need to arbitrarily identify the baseline around individual peaks for background subtraction. The spectral fitting method provides specific advantages, such as (1) quantification of signals from multiplex spectra with overlapping peaks, (2) robust removal of all background without introducing artifacts that occur from conventional background subtraction, (3) quantitative spot-by-spot assessment of the analysis error, (4) lack of operator bias, and (5) simple automated implementation appropriate for high-throughput analysis.

Multivariate spectral fitting methods, such as principle component analysis (PCA), and classification algorithms provide powerful tools for identifying key components in multichannel data. These methods have been very successful for analyzing the native Raman emission from tissues and cells.[31] PCA has been demonstrated for identification of signals from multiplex Raman probe mixtures;[32,33] however, the output may be difficult to interpret since components identified in the spectrum do not necessarily represent single probes. The simple spectral fitting approach presented here is more akin to conventional spectral analysis of fluorescent labels in that it uses known probe signatures to constrain the analysis and provides a single intensity value for each individual probe. Fitting of the sharp Raman peaks must conform to known reference spectra, while it allows freedom in fitting broad features from unknown background, including autofluorescence. Further, it can be easily implemented using common software.

In the current study, we used single-laser excitation and spectral analysis to quantify up to four probes in a small portion of the visible window (*i.e.*, ~40 nm), without reaching the limit of multiplexing. The COINs used here were optimized for green laser excitation, but the excitation wavelengths of Raman probes can be se-

lected based on nanoparticle material and structure,[10,34,35] the size of individual or clustered nanoparticles,[7,36] the molecular resonance of the Raman label,[19,36] or a combination of these parameters. As with molecular fluorophores (but not quantum dots), multiplexing levels can be increased by choosing probe sets with different optimal excitation wavelengths. For example, the molecular absorption effect was used in a system with two lasers (514 and 647 nm) to selectively excite certain Raman probes in multiplex nucleic acid assays,[18,19] and single gold nanoparticle probes have been optimized for longer wavelength excitation (785 nm).[10,18,23,27,35] Thus, distinct multiplex sets of Raman probes could be selectively excited by different lasers, with each spectral window providing high-order multiplexing. Spectral fitting and multiple laser excitation should allow simultaneous detection of more than 12 Raman probes in the near term and surpass the multiplexing capability of fluorescent probes.

Applications of Raman probes are strongly motivated by the potential for improved sensitivity and quantitation in multiplex applications. Autofluorescence in biological samples remains a challenge for analysis of fluorescent and Raman probes, and it is common to select excitation wavelengths in the red or near-infrared region to reduce autofluorescence intensity.[23,27] This wavelength restriction inherently reduces the number of probes that can be multiplexed since it only takes advantage of a small region of the spectrum. Spectral analysis provides specific advantages by (1) allowing quantitative separation of multiple probe signals, which maximizes multiplexing in a given wavelength region, and by (2) quantitatively separating probe signals from background autofluorescence, which extends the range of excitation wavelengths available in multiplex experiments. These benefits are particularly useful for improving quantitation and sensitivity in multiplex cell and tissue analyses, both *in vitro* and *in vivo*.

We demonstrate quantitative detection of up to four overlapping COIN signatures and the ability to detect weak COIN signals in the presence of interfering signals of 50−100-fold larger intensities. The imaging of FFPE tissue shown here represents one of the most challenging and clinically relevant applications for multiplex analysis. The spectral imaging method provides the tools that are urgently needed to realize the frequently cited potential of Raman probes for sensitive and quantitative multiplexing. The method is exceedingly simple to implement and can be easily adopted to improve quantitative multiplexing in any application of Raman probes.

METHODS

Plate Binding and Tissue Assays. AOH, NBA, and CVA were fabricated using a "hot" method,[7] and BFU, CEI, and TMR were fabricated using a "cold" method.[8] COINs were conjugated to anti-PSA antibody (antihuman Kallikrein 3; R&D Systems) or anticytokeratin-18 antibody (Abcam) by EDC coupling chemistry. Functionalized COINs are ~60 nm in diameter. Plate assays followed protocols described previously.[7,8,13] Briefly, purified PSA antigen (purified PSA from human semen, Sigma P3338) was adsorbed onto aldehyde slides (Nunc). COINs conjugated to anti-PSA antibodies (antihuman Kallikrein 3; R&D Systems AF1344) were incubated in wells, followed by washing and spectral measurement. Spectra were recorded from 225 points in each well. For tissue staining, 5 μm thick human prostate tissue sections were mounted on glass slides, deparaffinized, and rehydrated, followed by antigen retrieval using proteinase-K (5 min at room temperature, DakoS3020).[8,13] Both COINs were combined and incubated with the tissue in a single step, followed by incubation with YOYO-3 iodide nucleic acid stain (1:1000 dilution, 5 min incubation at room temperature; Invitrogen, Y3606). The sample was washed twice with PBST, rinsed with 0.1 M NaCl, and cover-slipped. The co-localization image in Figure 2D was generated from pure component images by color coding pixels that were positive for two analytes. Magenta pixels are positive for AOH (PSA) and YOYO (nuclei); yellow pixels are positive for AOH and BFU (CK18), but not for YOYO.

Raman Microscope Instrumentation. Spectral acquisition for plate assays, solution assays, and tissue assays used two similar instruments,[7,8] one with a 514 nm laser (plate and solution assays) and the other with a 532 nm laser (tissue assays). The location of Raman peaks (reported in wavenumber shift) is the same regardless of the excitation wavelength, and both green lasers effectively excite COIN. Each system used a conventional microscope equipped with an epi-illumination head to provide laser excitation and spectral acquisition, and spectra were acquired using a spectrograph and thermoelectrically cooled CCD detector. For tissue analysis, each spectrum was acquired with a 20× objective using 0.l s acquisition time and 650 μW laser power at the sample surface.

The Spectral Deconvolution Method. ***Reference Spectra.*** Spectra from single probe assays were collected in separate experiments with the same instrumentation and spectral resolution, so that reference spectra and measured spectra had a point-by-point correspondence. All probe reference spectra were normalized to a common intensity, for example

```
'COIN1referencespectrum =
   COIN1referencespectrum / mean(COIN1referencespectrum);'
```

Free-Fitting Polynomial. A polynomial was created by the combination of polynomial components of ascending order, and each polynomial component is included in the fitting method as an individual "reference spectrum". In Matlab (Mathworks), each polynomial component was created based on the wavenumber shift axis or pixel number axis (*e.g.*, 'poly0 = 1; poly1 = wnshift; poly2 = wnshift.^2; poly3 = wnshift.^3', where 'wnshift' is the wavenumber shift axis). Other functions could be substituted or combined to account for unusual spectral features in the background. All reference spectra were put into an array for easy handling (called 'referencespectra' below; an array of *n* reference spectra with *m* spectral points).

Analytical Methods. The spectral fitting procedure is a conventional nonlinear regression of the measured spectrum using the reference spectra described above. Descriptions below use a single spectrum for simplicity (called 'samplespectrum' below; spectrum with *m* spectral points), and large arrays are simply handled by looping the commands.

```
signals = regress(samplespectrum, referencespectra);'
```

The result consists of a list of signals, one for each component in the reference spectra set ('signals'; *n* values). The spectral fitting error is calculated as the percent difference between

measured and best-fit spectra averaged across the spectral fitting range.

```
'bestfitspectra = signals * referencespectra;'

'spectralfittingerror_points = abs(samplespectrum -
                    bestfitspectra) ./ samplespectrum * 100;'

'spectralfittingerror_mean = mean(spectralfittingerror_points);'
```

The point-by-point spectral fitting error is shown in Figure 2D, and the mean value across the fitting range provides a single value for the error in each measured spectrum.

Acknowledgment. The authors thank Intel Digital Health Group's Biomedical and Life Sciences research team for development and synthesis of COIN reagents. Data for the triplex solution assays were acquired by J. Zhu based on experimental design by K. Swartz. The authors thank K.-B. Sung for his role in development of COIN tissue analysis, and K. Adolphson at the Fred Hutchinson Cancer Research Center for contributions to development of COIN assay conditions. The authors thank M. Roth at the Fred Hutchinson Cancer Research Center for facilitating the collaboration and for inspiring project discussion. B.K. received support from the prostate SPORE (P50 CA97186) and the Cancer Center Grant (P30 CA015704).

Supporting Information Available: Example of polynomial components used in the spectral fitting method; summary statistics and quality measures for the triplex solution measurement of Figure 3; single COIN PSA plate binding assays corresponding to quadruplex plate binding assay of Figure 4; summary statistics and quality measures for singlet and quadruplex PSA plate binding assays of Figure 4; immunofluorescence image showing specificity of PSA and CK18 as markers for prostate epithelium; summary statistics and quality measures for triplex assays using BFU−CK18, AOH−PSA, and YOYO nucleic acid stain on FFPE prostate tissues in Figure 5; steric hindrance between COINs in tissue and plate multiplex assays. This material is available free of charge *via* the Internet at http://pubs.acs.org.

REFERENCES AND NOTES

1. Fleischmann, M.; Hendra, P. J.; McQuillan, A. J. Raman-Spectra of Pyridine Adsorbed at a Silver Electrode. *Chem. Phys. Lett.* **1974**, *26*, 163–166.
2. Albrecht, M. G.; Creighton, J. A. Anomalously Intense Raman-Spectra of Pyridine at a Silver Electrode. *J. Am. Chem. Soc.* **1977**, *99*, 5215–5217.
3. Jeanmaire, D. L.; Vanduyne, R. P. Surface Raman Spectroelectrochemistry. 1. Heterocyclic, Aromatic, and Aliphatic-Amines Adsorbed on Anodized Silver Electrode. *J. Electroanal. Chem.* **1977**, *84*, 1–20.
4. Moskovits, M. Surface-Enhanced Spectroscopy. *Rev. Mod. Phys.* **1985**, *57*, 783–826.
5. Kneipp, K.; Wang, Y.; Kneipp, H.; Perelman, L. T.; Itzkan, I.; Dasari, R.; Feld, M. S. Single Molecule Detection Using Surface-Enhanced Raman Scattering (SERS). *Phys. Rev. Lett.* **1997**, *78*, 1667–1670.
6. Nie, S. M.; Emery, S. R. Probing Single Molecules and Single Nanoparticles by Surface-Enhanced Raman Scattering. *Science* **1997**, *275*, 1102–1106.
7. Su, X.; Zhang, J.; Sun, L.; Koo, T. W.; Chan, S.; Sundararajan, N.; Yamakawa, M.; Berlin, A. A. Composite Organic−Inorganic Nanoparticles (COINs) with Chemically Encoded Optical Signatures. *Nano Lett.* **2005**, *5*, 49–54.
8. Sun, L.; Sung, K.-B.; Dentinger, C.; Lutz, B.; Nguyen, L.; Zhang, J.; Qin, H.; Yamakawa, M.; Cao, M.; Lu, Y.; et al. Composite Organic−Inorganic Nanoparticles as Raman Labels for Tissue Analysis. *Nano Lett.* **2007**, *7*, 351–356.
9. Grubisha, D. S.; Lipert, R. J.; Park, H. Y.; Driskell, J.; Porter, M. D. Femtomolar Detection of Prostate-Specific Antigen: An Immunoassay Based on Surface-Enhanced Raman Scattering and Immunogold Labels. *Anal. Chem.* **2003**, *75*, 5936–5943.
10. Ni, J.; Lipert, R. J.; Dawson, G. B.; Porter, M. D. Immunoassay Readout Method Using Extrinsic Raman Labels Adsorbed on Immunogold Colloids. *Anal. Chem.* **1999**, *71*, 4903–4908.
11. Driskell, J. D.; Kwarta, K. M.; Lipert, R. J.; Porter, M. D.; Neill, J. D.; Ridpath, J. F. Low-Level Detection of Viral Pathogens by a Surface-Enhanced Raman Scattering Based Immunoassay. *Anal. Chem.* **2005**, *77*, 6147–6154.
12. Cui, Y.; Ren, B.; Yao, J. L.; Gu, R. A.; Tian, Z. Q. Multianalyte Immunoassay Based on Surface-Enhanced Raman Spectroscopy. *J. Raman Spectrosc.* **2007**, *38*, 896–902.
13. Lutz, B.; Dentinger, C.; Sun, L.; Nguyen, L.; Zhang, J.; Chmura, A. J.; Allen, A.; Chan, S.; Knudsen, B. Raman Nanoparticle Probes for Antibody-Based Protein Detection in Tissues. *J. Histochem. Cytochem.* **2008**, *56*, 371–379.
14. Monaghan, P. B.; McCarney, K. M.; Ricketts, A.; Littleford, R. E.; Docherty, F.; Smith, W. E.; Graham, D.; Cooper, J. M. Bead-Based DNA Diagnostic Assay for Chlamydia Using Nanoparticle-Mediated Surface-Enhanced Resonance Raman Scattering Detection within a Lab-on-a-Chip Format. *Anal. Chem.* **2007**, *79*, 2844–2849.
15. Faulds, K.; Smith, W. E.; Graham, D. Evaluation of Surface-Enhanced Resonance Raman Scattering for Quantitative DNA Analysis. *Anal. Chem.* **2004**, *76*, 412–417.
16. Park, T.; Lee, S.; Seong, G. H.; Choo, J.; Lee, E. K.; Kim, Y. S.; Ji, W. H.; Hwang, S. Y.; Gweon, D. G.; Lee, S. Highly Sensitive Signal Detection of Duplex Dye-Labelled DNA Oligonucleotides in a PDMS Microfluidic Chip: Confocal Surface-Enhanced Raman Spectroscopic Study. *Lab Chip* **2005**, *5*, 437–442.
17. Cao, Y. W. C.; Jin, R. C.; Mirkin, C. A. Nanoparticles with Raman Spectroscopic Fingerprints for DNA and RNA Detection. *Science* **2002**, *297*, 1536–1540.
18. Stokes, R. J.; Macaskill, A.; Lundahl, P. J.; Smith, W. E.; Faulds, K.; Graham, D. Quantitative Enhanced Raman Scattering of Labeled DNA from Gold and Silver Nanoparticles. *Small* **2007**, *3*, 1593–1601.
19. Faulds, K.; McKenzie, F.; Smith, W. E.; Graham, D. Quantitative Simultaneous Multianalyte Detection of DNA by Dual-Wavelength Surface-Enhanced Resonance Raman Scattering. *Angew. Chem., Int. Ed.* **2007**, *46*, 1829–1831.
20. Cao, Y. C.; Jin, R. C.; Nam, J. M.; Thaxton, C. S.; Mirkin, C. A. Raman Dye-Labeled Nanoparticle Probes for Proteins. *J. Am. Chem. Soc.* **2003**, *125*, 14676–14677.
21. Bonham, A. J.; Braun, G.; Pavel, I.; Moskovits, M.; Reich, N. O. Detection of Sequence-Specific Protein−DNA Interactions *via* Surface Enhanced Resonance Raman Scattering. *J. Am. Chem. Soc.* **2007**, *129*, 14572–14573.
22. Lee, S.; Kim, S.; Choo, J.; Shin, S. Y.; Lee, Y. H.; Choi, H. Y.; Ha, S. H.; Kang, K. H.; Oh, C. H. Biological Imaging of HEK293 Cells Expressing PLC Gamma 1 Using Surface-Enhanced Raman Microscopy. *Anal. Chem.* **2007**, *79*, 916–922.
23. Huang, X. H.; El-Sayed, I. H.; Qian, W.; El-Sayed, M. A. Cancer Cells Assemble and Align Gold Nanorods Conjugated to Antibodies to Produce Highly Enhanced, Sharp, and Polarized Surface Raman Spectra: A Potential Cancer Diagnostic Marker. *Nano Lett.* **2007**, *7*, 1591–1597.
24. Schlucker, S.; Kustner, B.; Punge, A.; Bonfig, R.; Marx, A.; Strobel, P. Immuno-Raman Microspectroscopy: *In Situ* Detection of Antigens in Tissue Specimens by Surface-Enhanced Raman Scattering. *J. Raman Spectrosc.* **2006**, *37*, 719–721.
25. Yu, K. N.; Lee, S.-M.; Han, J. Y.; Park, H.; Woo, M.-A.; Noh, M. S.; Hwang, S.-K.; Kwon, J.-T.; Jin, H.; Kim, Y.-K.; et al. Multiplex Targeting, Tracking, and Imaging of Apoptosis by Fluorescent Surface Enhanced Raman Spectroscopic Dots. *Bioconjugate Chem.* **2007**, *18*, 1155–1162.
26. Kim, J.-H.; Kim, J.-S.; Choi, H.; Lee, S.-M.; Jun, B.-H.; Yu, K.-N.; Kuk, E.; Kim, Y.-K.; Jeong, D. H.; Cho, M.-H.; Lee, Y.-S. Nanoparticle Probes with Surface Enhanced Raman Spectroscopic Tags for Cellular Cancer Targeting. *Anal. Chem.* **2006**, *78*, 6967–6973.
27. Qian, X. M.; Peng, X.-H.; Ansari, D. O.; Yin-Goen, Q.; Chen, G. Z.; Shin, D. M.; Yang, L.; Young, A. N.; Wang, M. D.; Nie, S.

In vivo Tumor Targeting and Spectroscopic Detection with Surface-Enhanced Raman Nanoparticle Tags. *Nat. Biotechnol.* **2008**, *26*, 83–90.
28. Faulds, K.; Barbagallo, R. P.; Keer, J. T.; Smith, W. E.; Graham, D. SERRS as a More Sensitive Technique for the Detection of Labelled Oligonucleotides Compared to Fluorescence. *Analyst* **2004**, *129*, 567–568.
29. Levenson, R. M.; Mansfield, J. R. Multispectral Imaging in Biology and Medicine: Slices of Life. *Cytometry A* **2006**, *69A*, 748–758.
30. Doering, W. E.; Piotti, M. E.; Natan, M. J.; Freeman, R. G. SERS as a Foundation for Nanoscale, Optically Detected Biological Labels. *Adv. Mater.* **2007**, *19*, 3100–3108.
31. Hanlon, E. B.; Manoharan, R.; Koo, T. W.; Shafer, K. E.; Motz, J. T.; Fitzmaurice, M.; Kramer, J. R.; Itzkan, I.; Dasari, R. R.; Feld, M. S. Prospects for *in vivo* Raman Spectroscopy. *Phys. Med. Biol.* **2000**, *45*, R1–R59.
32. McCabe, A. F.; Eliasson, C.; Prasath, R. A.; Hernandez-Santana, A.; Stevenson, L.; Apple, I.; Cormack, P. A. G.; Graham, D.; Smith, W. E.; Corish, P.; et al. SERRS Labelled Beads for Multiplex Detection. *Faraday Discuss.* **2006**, *132*, 303–308.
33. Watson, D. A.; Brown, L. O.; Gaskill, D. R.; Naivar, M.; Graves, S. W.; Doorn, S. K.; Nolan, J. P. A Flow Cytometer for the Measurement of Raman Spectra. *Cytometry A* **2008**, *73A*, 119–128.
34. Mulvaney, S. P.; Musick, M. D.; Keating, C. D.; Natan, M. J. Glass-Coated, Analyte-Tagged Nanoparticles: A New Tagging System Based on Detection with Surface-Enhanced Raman Scattering. *Langmuir* **2003**, *19*, 4784–4790.
35. Schwartzberg, A. M.; Olson, T. Y.; Talley, C. E.; Zhang, J. Z. Synthesis, Characterization, and Tunable Optical Properties of Hollow Gold Nanospheres. *J. Phys. Chem. B* **2006**, *110*, 19935–19944.
36. Cunningham, D.; Littleford, R. E.; Smith, W. E.; Lundahl, P. J.; Khan, I.; McComb, D. W.; Graham, D.; Laforest, N. Practical Control of SERRS Enhancement. *Faraday Discuss.* **2006**, *132*, 135–145.